ORIGINAL RESEARCH

LKB1 Knockout Mouse Develops Spontaneous Atrial Fibrillation and Provides Mechanistic Insights Into Human Disease Process

Cevher Ozcan, MD; Emily Battaglia, MD; Rebeccah Young, MA; Gen Suzuki, MD, PhD

***Background*—**Atrial fibrillation (AF) is a complex disease process, and the molecular mechanisms underlying initiation and progression of the disease are unclear. Consequently, AF has been difficult to model. In this study, we have presented a novel transgenic mouse model of AF that mimics human disease and characterized the mechanisms of atrial electroanatomical remodeling in the genesis of AF.

***Methods and Results*—**Cardiac-specific liver kinase B1 (LKB1) knockout (KO) mice were generated, and 47% aged 4 weeks and 95% aged 12 weeks developed spontaneous AF from sinus rhythm by demonstrating paroxysmal and persistent stages of the disease. Electrocardiographic characteristics of sinus rhythm were similar in KO and wild-type mice. Atrioventricular block and atrial flutter were common in KO mice. Heart rate was slower with persistent AF. In parallel with AF, KO mice developed progressive biatrial enlargement with inflammation, heterogeneous fibrosis, and loss of cardiomyocyte population with apoptosis and necrosis. Atrial tissue was infiltrated with inflammatory cells. C-reactive protein, interleukin 6, and tumor necrosis factor α were significantly elevated in serum. KO atria demonstrated elevated reactive oxygen species and decreased AMP-activated protein kinase activity. Cardiomyocyte and myofibrillar ultrastructure were disrupted. Intercellular matrix and gap junction were interrupted. Connexins 40 and 43 were reduced. Persistent AF caused left ventricular dysfunction and heart failure. Survival and exercise capacity were worse in KO mice.

***Conclusions*—**LKB1 KO mice develop spontaneous AF from sinus rhythm and progress into persistent AF by replicating the human AF disease process. Progressive inflammatory atrial cardiomyopathy is the genesis of AF, through mechanistic electrical and structural remodeling. **(*J Am Heart Assoc*. 2015;4:e001733 doi: 10.1161/JAHA.114.001733)**

Key Words: animal models of human disease remodeling • atrial fibrillation • atrium • inflammation • pathogenesis

Atrial fibrillation (AF) is a common sustained arrhythmia with increasing incidence and prevalence over time.[1–4] It is associated with high risk of all-cause mortality, morbidity, and recurrent hospitalization.[1,5–17] Despite the magnitude of the disease, there is no effective strategy for primary and secondary prevention of AF. Understanding the exact mechanisms responsible for the disease process is essential for developing strategies for prevention and treatment of the disease, particularly early preclusion[1,17,18]; however, the molecular and cellular mechanisms for initiation, maintenance, and progression of the AF disease process are not known.

Development of AF is a complex pathophysiological process associated with multiple risk factors including systemic and structural heart disease and genetic susceptibility.[1,9,13–17] Initiation and progression of AF require vulnerable atrial substrate and electrophysiological triggers.[1,19–22] Structural substrate of AF is reported to involve atrial dilation, stretch, fibrosis, loss of muscle mass, amyloidosis, extracellular matrix remodeling, and disruption of gap junctions.[1,9,13–22] Electrical substrate includes abnormal automaticity, triggered activity, or multiple reentrant wavelets.[1,19–23] A vulnerable substrate develops with heterogeneous shortening of the atrial effective refractory period, ion channel remodeling, and altered conduction velocity in association with change in resting membrane potential and ionic current in atrial myocytes[19–25]; however, exact causes of electrical and structural substrate at the cellular level are not known. In addition, the causal relationship between structural and electrical substrate in AF and the role of inflammation in this process are not clearly established.[1,19–25] We hypothesize

From the Division of Cardiovascular Medicine, Department of Medicine, Clinical & Translational Research Center, University at Buffalo School of Medicine and Biomedical Sciences, Buffalo, NY (C.O., E.B., R.Y., G.S.); Section of Cardiology, Department of Medicine, University of Chicago, IL (C.O.).

Correspondence to: Cevher Ozcan, MD, Section of Cardiology, University of Chicago, 5841 S. Maryland Avenue, MC 6080, Room B608, Chicago, IL 60637. E-mail: cozcan@uchicago.edu

Received December 18, 2014; accepted January 14, 2015.

that atrial myocardial inflammation and development of atrial cardiomyopathy play major roles in the genesis of AF by creating electroanatomical substrate for initiation and progression of the AF disease process.

Animal models are critical to study mechanisms of disease and to design new therapies for prevention and treatment.[1,23–25] It has been difficult to model AF because of the complexity of the disease process. To date, several small and large animal models have been studied for AF.[23–25] Initially, AF was induced in normal hearts using vagal nerve stimulation or acetylcholine infusion.[26] Subsequently, disease conditions such as pericarditis, heart failure, ischemia, or tachycardia were used to induce AF in animals.[23–25] In recent years, genetically modified hearts became preferred for experimental models of AF to evaluate the functional significance of this modification. Current AF models, however, are associated with numerous limitations including lower incidence of AF, variability of results, lack of reproducibility, and inefficiency in short- and long-term remodeling. In addition, these models failed to match the human AF disease process. Recently, AF was documented in mice with deletion of liver kinase B1 (LKB1) without characterization of the AF disease process and electroanatomical properties.[27] In this paper, we define a novel transgenic mouse model of AF, cardiac-specific LKB1 knockout (KO), with spontaneous development of AF and mechanistic electroanatomical changes within the atria that mimic the human disease process.

Methods

The University at Buffalo animal care and use committee reviewed and approved this research protocol and the experimental procedures. The procedures followed were in accordance with institutional guidelines. In addition, all experiments were performed in accordance with the *Guide for the Care and Use of Laboratory Animals*, published by the US National Institutes of Health (National Institutes of Health publication no. 5377-3, 1996).

Animals

Cardiac-specific LKB1 KO mice (*C57BL/6*) were generated by crossing LKB1$^{flox/flox}$ mice with transgenic mice expressing Cre-recombinase from the major histocompatibility complex promoter, as reported previously.[27,28] Transgenic mice were confirmed to be lacking LKB1 in myocytes by polymerase chain reaction and Western blot analysis before the experiments. Wild-type (WT) mice were of the same strain as the corresponding transgenic mice (Jackson Laboratory, Bar Harbor, ME, USA). During experimental procedures, mice were anesthetized by using 0.5% to 2.5% isoflurane for deep anesthesia and/or termination.[29] The adequacy of anesthesia was monitored continuously, and the isoflurane dose was adjusted to maintain optimal anesthesia during the procedure. In addition, subcutaneous injections of buprenorphine (0.1 mg/kg) and carprofen (10 mg/kg) were given perioperatively for analgesia. Male KO mice were used in all experiments, in comparison with age- and sex-matched WT mice.

Electrophysiology

Continuous electrocardiographic monitoring (PowerLab using LabChart software; ADInstruments) was performed periodically on weaning mice aged 3 weeks. Subcutaneous 29-gauge needle electrodes were placed in the limbs for lead II position. Heart rate (HR), rhythm, and conduction intervals were recorded and analyzed from limb leads. In addition, an ECG telemetry system (TA11ETA-F10 implantable radio frequency transmitter for ECG; Data Sciences International Inc) was implanted subcutaneously at posterior neck and chest in mice aged 4 to 5 weeks.[30,31] Leads were tunneled to the anterior chest in lead II position. After recovery, data were sampled in caged, moving mice. Ambulatory heart rhythm and HR were monitored continuously. The incidence and type of arrhythmias (AF, atrioventricular block [AVB], premature contractions, supraventricular tachycardia, ventricular tachycardia, and ventricular fibrillation) were evaluated on ECG and telemetry recordings. AF was described as paroxysmal AF (PAF) or persistent AF (persAF). PAF was defined as spontaneous conversion of AF to sinus rhythm (SR) documented during telemetry or EKG recordings. PersAF was identified if a mouse was continuously in AF with no documented conversion to SR during monitoring by telemetry and EKG recordings. Sinus node function and intrinsic HR were evaluated with intraperitoneal administration of atropine (1 mg/kg) and then metoprolol (4 mg/kg) while mice were in SR. Surface ECG was recorded continuously when the parasympathetic and sympathetic autonomic responses were blocked with injection of atropine and metoprolol.[31,32]

Imaging

In vivo cardiac structure and function were evaluated by echocardiogram (Vivid E9 17-in 2-dimensional BT12 mouse echo probe, model I13L, 5.8 to 14 MHz; General Electric Inc) and cardiac magnetic resonance imaging (MRI; 9.4-T scanner; Bruker) while animals were under light anesthesia with isoflurane.[29–34] Two-dimensionally guided M-mode images of the left ventricle (LV) were acquired in the long and short axes to assess LV cavity dimensions, anterior and posterior wall thicknesses, and fractional shortening. Cardiac MRI data acquisition was performed with cardiorespiratory gating in the 4-chamber (horizontal long axis), 2-chamber (vertical long

axis), and short-axis planes at multiple slice locations.[33] Right and left atrial areas and diameters were measured by cardiac MRI at maximal size in the phase of the cardiac cycle. The measurements were done in 2- and 4-chamber views at longitudinal and transverse diameters.[34] Gross anatomy of the heart was evaluated after rapid excision following anterior thoracotomy. Hearts were fixed in 10% formaldehyde solution and cut into thin sections and stained with hematoxylin and eosin for evaluation.[29,35]

Histopathology

Atrial and ventricular tissue samples were stained with Masson's trichrome and hematoxylin and eosin for histopathological analysis by light microscopy (Nikon Eclipse E600).[29,35] Connective tissue was quantified in Masson's trichrome-stained sections. Cardiomyocyte and intercellular ultrastructures were visualized using electron microscopy (JEOL FX1200) after fixation of hearts in EM-grade glutaraldehyde solution.[29,35] Apoptosis in atrial tissue was quantified using fluorescent terminal deoxynucleotidyl transferase-mediated dUTP nick-labeling, or TUNEL, staining (Chemicon Inc), as described.[36] Sections were also incubated with antibodies to cardiac troponin I (cTnI; Santa Cruz Biotechnology, Inc) to detect colocalization in myocytes. Nuclei were stained with 4′,6-diamidino-2-phenylindole (DAPI, Vectasheild; Vector Laboratories). Ten fields (4.6 mm^2) per sample were randomly selected, and images were acquired with an AxioImager equipped with ApoTome (Zeiss). Apoptosis-positive myocytes and nonmyocytes were counted as positive nuclei per square millimeter in each sample.

Immunoblot

Right and left atrial tissue samples were used for Western blotting.[29,35] Connexin 40 (Millipore), connexin 43 (Cell Signaling Technology, Inc), AMP-activated protein kinase α (AMPKα; Cell Signaling Technology, Inc), and caspase 3 and 9 (Cell Signaling Technology, Inc) antibodies were used and visualized with enhanced chemiluminescence. SYPRO Ruby (Life Technologies), total protein blot staining, and an antibody against GAPDH were used as loading controls. Bands were quantified with the Bio-Rad Chemi-Doc gel imager and Image Lab software. The results are presented as a ratio for total protein.

Cytokines

Serum samples of mice were collected and analyzed for circulating cytokines including interleukin 6 (IL-6), tumor necrosis factor α (TNF-α), and C-reactive protein (CRP), with a Luminex 100/200 system (Luminex Inc). Enzyme-linked immunosorbent assay kits (Mouse Cytokine/Chemokine Magnetic Bead Panel Kit; Millipore) were used for the measurements.

Oxidative Stress

Reactive oxygen species were measured with 2′,7′-dichlorofluorescein diacetate fluorescence (Sigma-Aldrich) in atrial tissue. Reactive oxygen species cause oxidation of 2′,7′-dichlorodihydrofluorescein, yielding the fluorescent product 2′,7′-dichlorofluorescein, which quantifies hydrogen peroxide. Atrial tissue (100-μg protein) was incubated with 100 μmol/L 2′,7′-dichlorofluorescein, and the fluorescence was measured using a spectrofluorometer at 480-nm excitation and 530-nm emission, as defined previously.[29]

Exercise Capacity

KO and WT mice were simultaneously exercised with increases of velocity at 1-minute intervals on a 6-track treadmill with a rear shock grid to enforce running (stimulatory shock of 0.46 mA; Columbus Instruments).[37] Mice were compared in terms of total distance run and time before dropout when accelerated from 5 m/min to a maximum of 15 m/min over 10 minutes and at 0° to 10° angle incline, with a total of 4 trials over 2 days. Failure to exercise despite 15 total shocks or 10 visits to the grid defined time of dropout.

Statistical Analysis

Data are presented as mean±SD, and sample size represents the number of animals used for experiments. Comparisons between groups were performed by parametric and nonparametric tests including the Student *t* test, ANOVA, and the Wilcoxon test. Survival was estimated by the Kaplan–Meier method. Terminated mice were excluded from survival analysis. A value of $P<0.05$ was considered statistically significant.

Results

Incidence of AF

Serial ECG and implantable telemetry recordings were completed in KO (n=34) and WT (n=20) mice for electrophysiological analysis. LKB1 KO mice were born in SR (Figure 1A, upper panel), and then 47% developed spontaneous AF at 4 weeks. Spontaneous AF was detected in 74% of KO mice aged 6 weeks (Figure 1A and 1B). Although no AF was documented in WT mice, 95% of KO mice developed AF by 12 weeks (Figure 1B). To our knowledge, this is the highest incidence of AF in surviving animal models of AF in the literature. During the first 4 to 6 weeks of diagnosis, AF was predominantly paroxysmal (Figure 1A, middle) and then

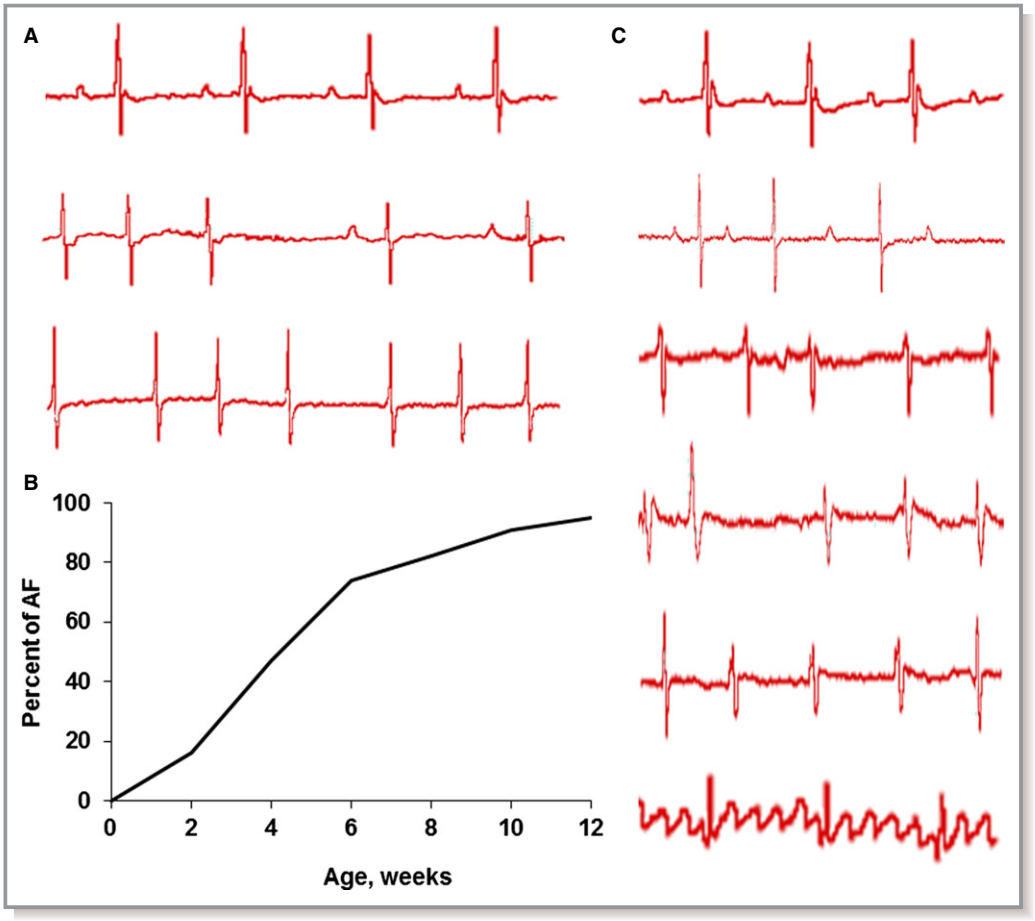

Figure 1. Electrophysiological characteristics. Electrocardiogram shows that liver kinase B1 (LKB1) knockout mice have sinus rhythm at birth (upper panel) and develop spontaneous paroxysmal AF (middle). Paroxysmal AF progressed into persistent AF (lower) (A). Incidence of AF was significantly high in LKB1 knockout mice and increased with age (n=34). AF occurred in the majority of knockout mice within 3 months (B). Various rhythm disorders were documented in knockout hearts including atrioventricular block (first and second degree, upper panels), premature atrial contractions (middle), intermittent bundle branch block, and atrial flutter (lower) (C). AF indicates atrial fibrillation.

progressed to a persAF stage (Figure 1A, lower). Frequency of conversion from PAF to persAF was 6.5% over 6 weeks; however, some KO mice developed persAF more rapidly, as did 41% aged 6 weeks.

In addition to AF, KO mice demonstrated variable heart rhythm disorders including first- and second-degree AVB, bundle branch block, premature atrial and ventricular contractions, and atrial flutter (Figure 1C). The most common conduction disease was first-degree AVB with profoundly prolonged PR interval from a mean of 37±3 to 50±6 ms (Figure 1C, upper left). In contrast, no arrhythmia or conduction disease was documented in WT mice.

Heart Rate, Conduction Intervals, and Other Arrhythmias

ECG characteristics were similar in KO (n=34) and WT (n=20) hearts in SR (Table 1). HR was comparable in both groups at 479±51 beats per minute (bpm) in KO mice and 495±72 bpm in WT mice ($P>0.05$). When KO mice developed PAF, HR remained unchanged (460±38 bpm) compared with KO in SR and WT mice ($P>0.05$); however, HR became slower (372±55 bpm, $P<0.001$) as PAF progressed into persAF over time. Progressively prolonged R-R interval in persAF and bradycardia (<300 bpm) developed in chronic persAF (Table). Moreover, ECG analysis showed comparable PR, QRS, and QTc intervals in WT and KO mice in SR ($P>0.05$). In SR and PAF, P-wave duration and amplitude were also similar in both groups ($P>0.05$). In PAF, PR interval and duration of ventricular electrical activation (QRS) were found to be longer compared with WT ($P<0.05$). KO mice with persAF showed wider QRS and longer QTc intervals than WT mice ($P<0.05$). Furthermore, sinus node function was evaluated in KO and WT mice by using sympathetic and parasympathetic blockage with atropine and metoprolol. KO mice were able to accelerate HR by 44% of baseline after administration of atropine

Table 1. Electrocardiographic Characteristics of the Mouse Model of Atrial Fibrillation

ECG Characteristics	WT (n=20)	KO-Sinus (n=34)	KO-PAF (n=15)	KO-PersAF (n=13)	*P* Value WT vs KO-Sinus	WT vs KO-PAF	WT vs KO-PersAF
R-R, ms	123±16	128±18	133±11	169±28	0.5	0.1	0.001
PR interval, ms	35.4±2	36.5±3	37.7±2	N/A	0.3	0.04	N/A
P-wave duration, ms	14.7±3	12.8±2	13.8±1	N/A	0.07	0.8	N/A
P-wave amplitude, mV	60±12	64±9	58±13	N/A	0.7	0.4	N/A
QRS duration, ms	7.9±1	8.3±1	10.7±2.7	12±2	0.3	0.02	<0.001
QTc interval, ms	38±4	46±11	95±13	96±17	0.2	<0.001	<0.001

KO indicates knockout; N/A, not applicable; PAF, paroxysmal atrial fibrillation; persAF, persistent atrial fibrillation; WT, wild type.

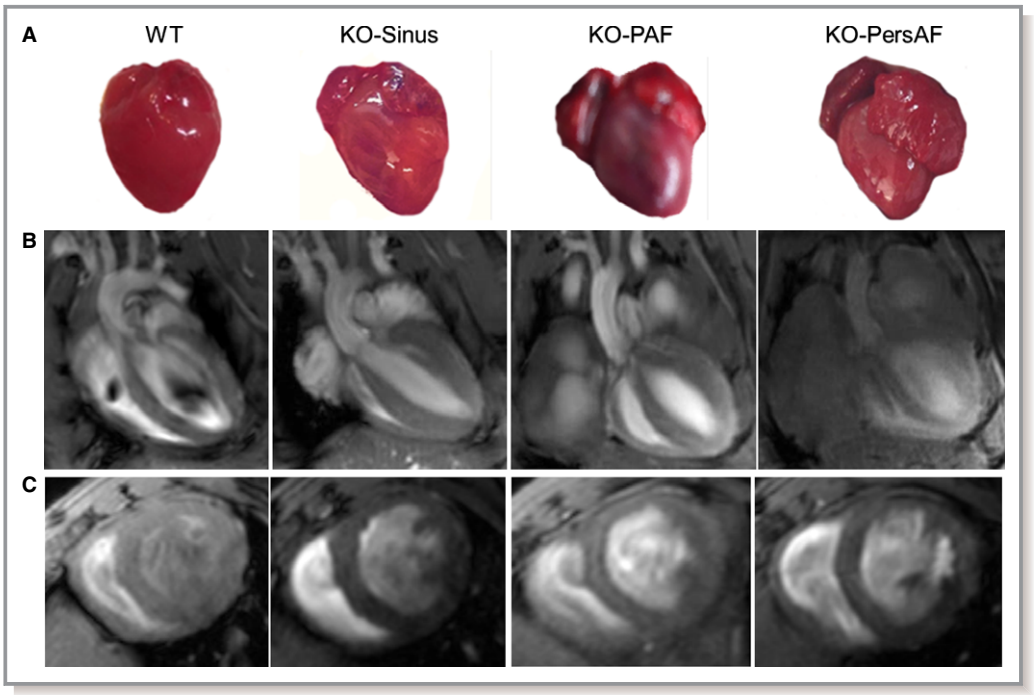

Figure 2. Cardiac structure. Cardiac magnetic resonance imaging (A) and gross anatomy (B) show significant enlargement of right and left atrial size in liver kinase B1 (LKB1) KO mouse heart compared with WT heart (n=4 in each group). Biatrial dilation progressively worsens in PAF and persAF; however, left ventricular size in LKB1 knockout mouse heart was similar to that of WT heart (C). KO indicates knockout; PAF, paroxysmal atrial fibrillation; persAF, persistent atrial fibrillation; WT, wild type.

(n=5), whereas WT mice increased HR by 31% (n=5). Consequently, there was no evidence of sinus node dysfunction in KO and WT hearts. Intrinsic HR in the presence of sympathetic and parasympathetic blockage (371±46 bpm in KO mice and 356±31 bpm in WT, $P>0.05$) was comparable in both groups.

Phenotype and Cardiac Structure

In SR or PAF, LKB1 KO and WT mice have similar phenotypes. Total body weight was comparable at 4 weeks (15.3±5 g in KO versus 12.8±1.4 g in WT, $P>0.05$) and 8 weeks (25.5±2.4 g in KO versus 24.4±1.3 g in WT, $P>0.05$). KO mice with persAF gained significant weight (mean of 30.7±3.8 g), whereas WT mice kept stable body weight (26.1±0.1 g) ($P<0.05$). Weight gain in persAF was associated with clinical signs of heart failure including evidence of peripheral edema and echocardiographic findings of pleural and pericardial effusions.

Cardiac structure in KO hearts was different than that in WT hearts by cardiac MRI, gross anatomy of excised heart, and echocardiogram (Figure 2). Right ventricular and LV chamber sizes were similar in WT and KO hearts in SR and PAF (Figures 2 and 3). LV systolic function was preserved

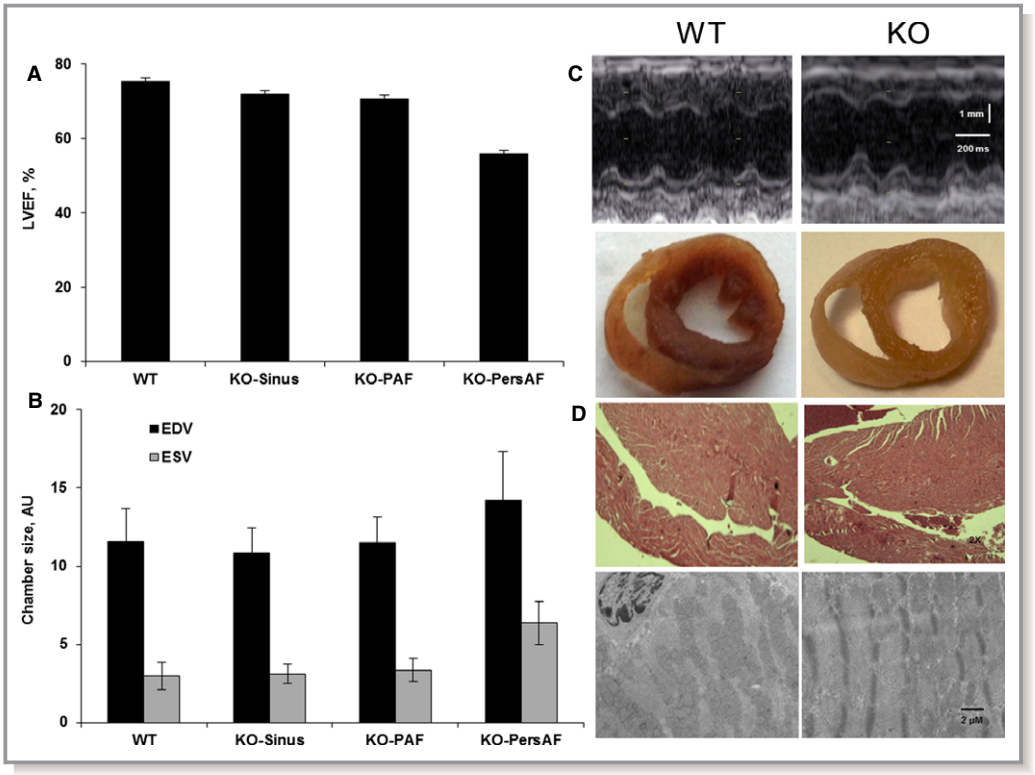

Figure 3. Ventricular structure and function. In sinus rhythm and PAF, LVEF (A) and chamber size (ESV and EDV) (B) in liver kinase B1 (LKB1) KO mouse heart were similar to those in WT heart; however, LVEF was significantly reduced in PersAF, and left ventricular end-systolic size was enlarged (n=4 in each group). Echocardiogram (C, upper) (n=7 in each group) and gross anatomy (C, lower) (n=6 in each group) confirmed these findings. Histology of the ventricular myocardium with hematoxylin and eosin staining by light microscopy (D, upper) and cardiomyocyte ultrastructure by electron microscopy (D, lower) in KO heart showed no significant difference compared with WT heart (n=4 in each group). Cellular and myofibrillar structures were organized. AU indicates arbitrary unit; EDV, end-diastolic volume; ESV, end-systolic volume; KO, knockout; LVEF, left ventricular ejection fraction; PAF, paroxysmal atrial fibrillation; PersAF, persistent atrial fibrillation; WT, wild type.

in KO mice with SR and PAF. LV ejection fraction was comparable between WT heart (75±4%) and KO heart in SR (72±2%) and in PAF (71±5%) (n=4 in each group, $P>0.05$ for all groups) (Figure 3A). PersAF was associated with significant LV dysfunction (LV ejection fraction 56±4%; $P<0.001$) (Figure 3A). LV end-diastolic and end-systolic diameter and volume were similar in WT and KO hearts in SR and PAF (Figure 3B); however, end-systolic area was larger in persAF compared with WT, SR, and PAF (n=4 in each group, $P<0.05$ for all groups) (Figure 3B). MRI, echocardiogram, and gross anatomy of the hearts showed no evidence of ventricular hypertrophy (Figures 2C and 3C). LV posterior wall (0.094±0.001 versus 0.098±0.002 cm) and interventricular septum thickness (0.093±0.001 versus 0.095±0.001 cm) were normal in KO and WT mice, respectively ($P<0.05$). Ventricular myocardium and cardiomyocyte evaluation by light (upper) and electron (lower) microscopy showed no significant tissue pathology in intercellular or cellular structure (Figure 3D).

The most remarkable difference was observed in atrial size (Figures 2 and 4). Right and left atria were significantly enlarged in KO heart starting in SR and progressively worsening in PAF and persAF (Figures 2A and 2B, 4). Right and left atrial sizes were measured by MRI in longitudinal 4-chamber view and short-axis horizontal view at maximum dimensions (Figure 4A through 4C). In SR, sizes of right (9.5±0.5 arbitrary unit (AU)) and left (9.5±0.5 AU) atria in KO heart were significantly larger than WT right (6.7±0.8 AU) and left (6.9±0.8 AU) atria in means of long and short axes and in individual measurement of long and short axes, as shown (n=4, $P<0.05$). In addition, MRI showed significantly increased atrial volume with development of PAF (right atrium: 16.8±5.3 AU, left atrium: 15.8±4.9 AU) and then progression of PAF to persAF (right atrium: 26.9.8±4.8 AU, left atrium: 25.1±4.2 AU) (n=4, $P<0.05$) (Figure 4A through 4C). In parallel, atrial weight was significantly higher in LKB1 KO mice in PAF (17±3 mg) and in persAF (33±6 mg) compared with atria of WT mice (10±3 mg) ($P<0.05$).

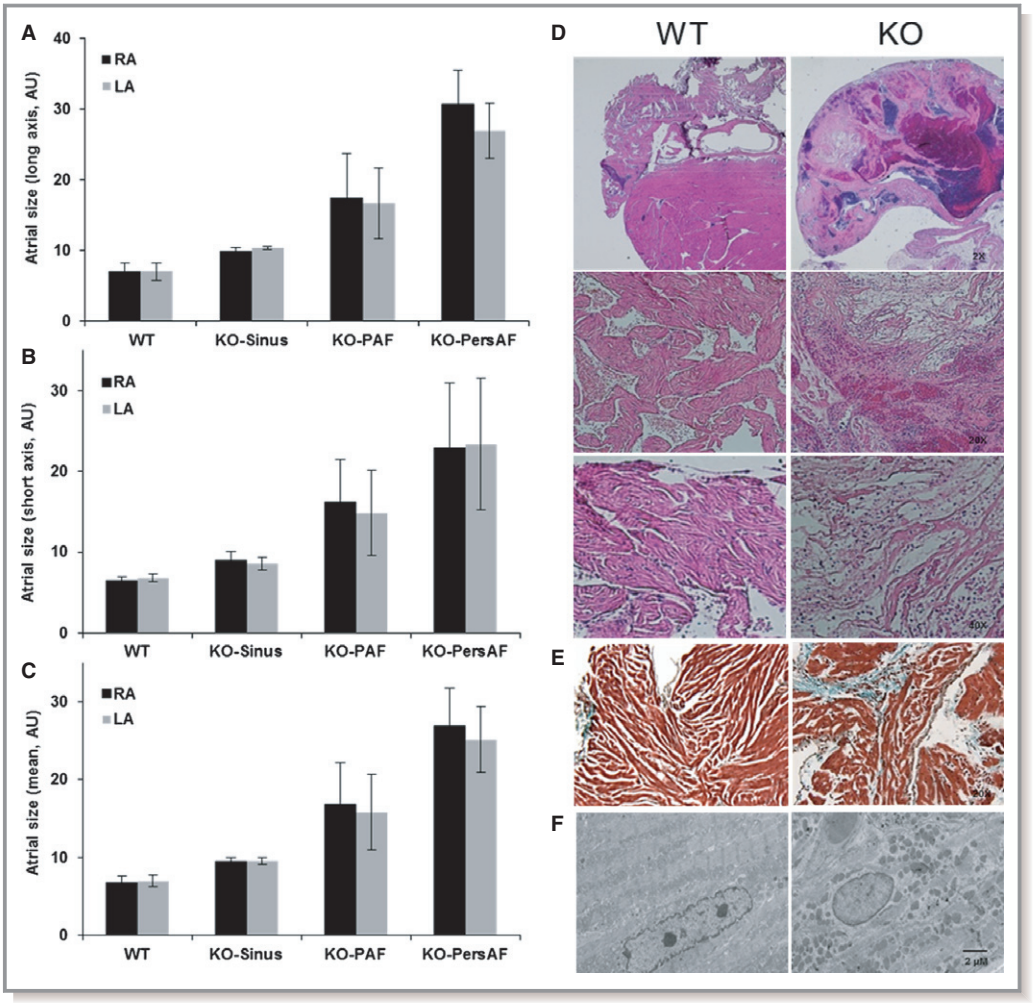

Figure 4. Atrial structure and histopathology. RA and LA enlargement was remarkable in liver kinase B1 (LKB1) KO mice in atrial fibrillation when compared with WT mice based on quantification by cardiac magnetic resonance imaging (n=4 in each group). RA and LA size was quantified based on long axis (A), short axis (B), and a collection of all views (mean) (C) while LKB1 KO mice were in sinus rhythm, PAF, and persAF in comparison to WT mice. Atrial tissue staining with hematoxylin and eosin showed dilated atrium (upper) with intra-atrial thrombus in comparison to WT (D) (n=4 in each group). There was disruption of intercellular structures and infiltration of inflammatory cells including lymphocytes, neutrophils, and macrophages in LKB1 KO heart (middle and lower). Increased extracellular deposition of other compounds were evident. Masson's trichrome staining showed that cardiomyocytes were replaced with fibrosis in AF in heterogeneous distribution (n=5) (E). Electron microscopy showed significantly altered ultrastructure of atrial myocytes by including disorganization of myofibrillar and organelle structures, disrupted mitochondria, and increased intracellular and extracellular deposition (F). AU indicates arbitrary unit; KO, knockout; LA, left atrial; PAF, paroxysmal atrial fibrillation; persAF, persistent atrial fibrillation; RA, right atrial; WT, wild type.

Histopathology of Atria

Atrial enlargement was found to be associated with significant inflammation and ultrastructural changes in atrial myocardium and cardiomyocyte (Figure 4D through 4F). Histological evaluation of atrial tissue samples in hematoxylin and eosin staining showed dilated atrium with thrombus (Figure 4D, upper), prominent intercellular disruption, and noncardiomyocyte cell infiltration and disorganization (Figure 4D, middle and lower). Atrial myocardium in KO mice demonstrated significant active inflammatory processes with infiltration of lymphocytes, neutrophils, and macrophages in contrast to WT atrium. Inflammatory cell infiltration and elevation of systemic inflammatory mediators were started in LKB1 KO atria in SR and then exacerbated in PAF and persAF. Intercellular matrix was also disrupted with this infiltration. Heterogeneous

fibrosis was significantly increased in KO atria compared with WT, as shown by Masson's trichrome staining (Figure 4E). Patchy fibrosis in KO atria started in SR (28%) and continued to build in PAF (32%) and persAF (34%) (n=5); however, fibrosis in WT atrial tissue was only 4% (n=4, $P<0.05$). Electron microscopy demonstrated cardiomyocyte ultrastructural deformation, with myofibrillar disorganization, sarcomere disarray, and organelle disruption in KO atria compared with WT atria (Figure 4F).

Quantification of myocyte and nonmyocyte cell populations in atria demonstrated significant differences between WT and KO hearts in persAF, as shown in cTnI and DAPI staining (n=6) (Figure 5A and 5B). The cardiomyocyte population was reduced (44%) in persAF ($P<0.05$). Noncardiomyocyte cells (56%) replaced atrial cardiomyocytes in the tissue. Catastrophic loss of myocytes occurred through apoptosis and necrosis. In KO atria, there was a 6-fold increase in TUNEL-positive nuclei in comparison to WT atria (n=6, $P<0.05$) (Figure 5C and 5D). Apoptosis started in SR and continued in PAF and persAF in KO atria. It occurred most prominently in KO sinus. In addition, cell-to-cell coupling was disrupted in KO atria with remodeling of extracellular matrix and reduced gap junction proteins such as connexin 40 (0.24±0.03 versus 0.82±0.01 AU) and connexin 43 (1.4±0.1 versus 14.4±1 AU) (n=5, $P<0.05$) (Figure 5E and 5F).

Moreover, inflammatory parameters in KO mice serum were significantly elevated in parallel with ultrastructural and electrophysiological changes in atrial myocardium. CRP, IL-6, and TNF-α were markedly higher in KO mice with PAF (CRP: 6.5±0.6; IL-6: 55±12; TNF-α: 3.8±0.6 pg/mL) and persAF (CRP: 10.2±1.1; IL-6: 324±26; TNF-α: 5.3±1.5 pg/mL) compared with WT (CRP: 4.3±0.4; IL-6: 2.1±1.5; TNF-α: 2.1±0.8 pg/mL) (n=10, $P<0.05$) (Figure 6). KO mice developed progressively increasing levels of inflammatory mediator

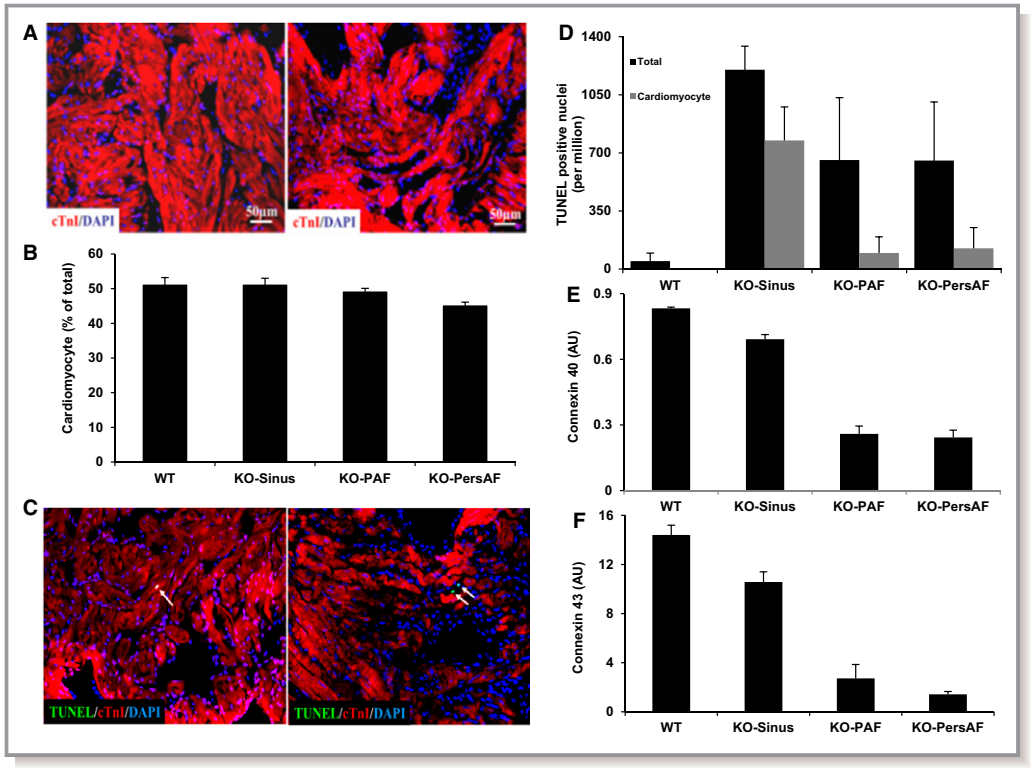

Figure 5. Atrial pathogenesis. Immunostaining of atrial tissue with cTnI to detect myocytes and DAPI for staining of nuclei showed that the cardiomyocyte cell population was significantly reduced in persAF (A) (n=6 in each group). Nonmyocyte cells were replaced by cardiomyocytes in atrial myocardium based on quantification of cells in collected images (B). The fluorescent TUNEL staining showed increased apoptosis in liver kinase B1 (LKB1) KO atrial cardiomyocytes while in sinus rhythm, PAF, or persAF compared with WT mouse atria (C) (n=6 in each group). Quantification of apoptosis showed more prominent apoptotic cells during initiation of atrial fibrillation than progression of PAF and persAF (D). Intercellular gap junction proteins were also disrupted, as demonstrated by immunoblotting of connexin 40 (E) and connexin 43 (F). In LKB1 KO heart, atrial myocardium contained lower connexin 40 and 43 in PAF and persPAF (n=5 in each group). Connexins 40 and 43 started to reduce in LKB1 KO heart while in sinus rhythm. AU indicates arbitrary unit; cTnI, cardiac troponin I; DAPI, 4′, 6-diamidino-2-phenylindole; KO, knockout; PAF, paroxysmal atrial fibrillation; persAF, persistent atrial fibrillation; TUNEL, terminal deoxynucleotidyl transferase-mediated dUTP nick-labeling; WT, wild type.

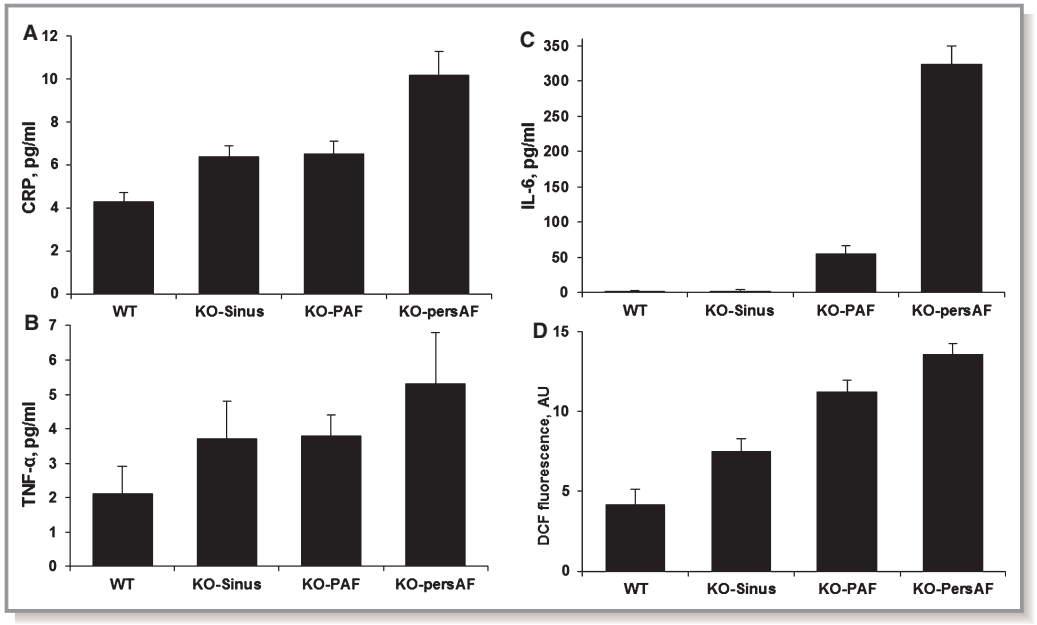

Figure 6. Inflammatory mediators. In addition to tissue evidence of inflammation, serum inflammatory markers were measured. CRP (A), TNF-α (B), and IL-6 (C) were found to be significantly elevated in liver kinase B1 (LKB1) KO mouse serum compared with WT mice. KO mice developed progressively increasing levels of inflammatory mediators starting in sinus rhythm (n=10 in each group). Mice with PAF or persAF have higher levels of inflammatory markers compared with KO mice in sinus rhythm. In parallel, DCF diacetate fluorescence demonstrated significant elevation of reactive oxygen species in LKB1 KO mouse atria (n=6 in each group) (D). Oxidative stress started in sinus rhythm and remained in PAF and persAF. AU indicates arbitrary unit; CRP, C-reactive protein; DCF, 2′,7′-dichlorofluorescein; IL-6, interleukin 6; KO, knockout; PAF, paroxysmal atrial fibrillation; persAF, persistent atrial fibrillation; TNF-α, tumor necrosis factor α; WT, wild type.

starting in SR (CRP: 6.4±0.5; IL-6: 2.2±1.2; TNF-α: 3.7±1 pg/mL). In persAF, inflammatory markers were at the highest level in the serum. Inflammation was associated with oxidative stress in atrial tissue. Reactive oxygen species (hydrogen peroxide) level was significantly elevated in LKB1 KO atria (13.6±0.7 AU) compared with WT (4.2±1 AU), as demonstrated by 2′,7′-dichlorofluorescein fluorescence (P<0.05) (Figure 6D). In addition, there was metabolic stress in LKB1 KO atria because LKB1 regulates AMPKα activation. Our measurement of phospho-AMPKα in atria of KO and WT mice showed significantly less activation of phospho-AMPKα in LKB1 KO atria (0.047±0.01 AU) compared with WT (0.028±0.005 AU) (P=0.02). Consequently, AF was associated with oxidative and metabolic stress that mediated inflammatory processes in atrial myocardium by causing dilated inflammatory atrial cardiomyopathy.

Exercise Capacity

KO mice in AF were unable to match the physical exertion of age- and sex-matched WT mice (Figure 7A and 7B). KO mice dropped out earlier from the treadmill test and at lower workloads than simultaneously exercised WT mice (n=7, P<0.05). KO mice in SR (9 minutes and 10 seconds) exercised longer than KO mice in PAF (4 minutes and 58 seconds) and persAF (4 minutes and 21 seconds) (n=4 to 6, P<0.05); however, WT mice (13 minutes and 49 seconds) exercised better than KO mice in SR or in PAF or persAF (n=7, P<0.001). In parallel, KO mice in SR (89±28 m) or PAF (35±4 m) and persAF (33±23.5 m) walked shorter distances than WT mice (159.5±52 m) on the treadmill with and without an amplified incline (P<0.05). Consequently, tolerated workload was lower in KO hearts.

Survival

LKB1 KO mice had increased mortality. Long-term survival was significantly worse in KO mice (94% at 6 weeks, 82% at 3 months, and 65% at 6 months), whereas there was no spontaneous death among WT mice during 6 months of observation (Figure 7C). Cause of death was most commonly heart failure and sudden cardiac death. Telemetry showed that ventricular fibrillation was the most immediate cause of death in mice with AF (Figure 7D). Ventricular

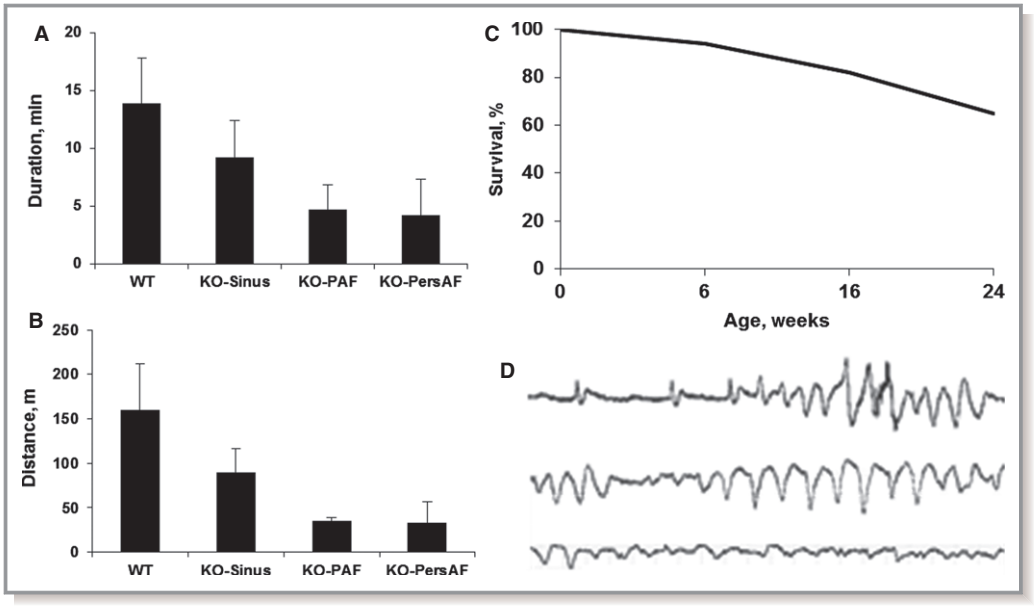

Figure 7. Stress tolerance and survival. Liver kinase B1 (LKB1) KO mice showed impaired functional status during the treadmill exercise stress test. Duration (A) and distance (B) of exercise capacity were significantly lower in sinus rhythm, PAF, and persAF (n=7 in each group). Long-term survival was also worse in LKB1 KO mice compared with WT mice (n=22 after excluding terminated mice) (C). A higher mortality rate was associated with atrial fibrillation and related heart failure. In addition, ventricular arrhythmia and tachycardia or fibrillation were documented as immediate causes of cardiac death (D). KO indicates knockout; PAF, paroxysmal atrial fibrillation; persAF, persistent atrial fibrillation; WT, wild type.

tachycardia, idioventricular rhythm, and torsade de pointes were other ventricular arrhythmias that proceeded to ventricular fibrillation and death. Consequently, heart failure, ventricular systolic dysfunction, exercise intolerance, and atrial myocardial remodeling contributed to poor survival in KO mice.

Another novel observation in LKB1 KO mice was higher incidence of peripartum cardiomyopathy. A total of 18.8% of female mice died during pregnancy as a result of cardiomyopathy. Within 2 weeks of postpartum monitoring, 76.9% of mice that had successfully given birth to litters died with heart failure at an average of 13.4 days postpartum. This is an important finding for understanding of the relationship between AF and peripartum cardiomyopathy.

Discussion

Our study presents several original findings. The LKB1 KO mouse is a novel small animal model of AF with 95% spontaneous development of AF within 3 months. The LKB1 KO mouse demonstrated characteristic progression of the AF disease process from SR to PAF and then persAF stages, as in humans, along with similar electrical and structural remodeling of atria. The genesis of AF included inflammatory atrial myocarditis in association with oxidative and metabolic stress that resulted in increased fibrosis, apoptosis, and disrupted ultrastructure. Myocarditis caused progressive atrial cardiomyopathy with significant biatrial enlargement and electrical and structural remodeling. As the structural substrate altered the electrical properties of atria, electrical remodeling triggered structural remodeling. Premature atrial contractions, AVB, and atrial flutter were predictors of AF in this model. AF caused LV dysfunction and heart failure and impaired survival and exercise capacity. AF increased the risk of peripartum cardiomyopathy and related mortality in LKB1 KO heart.

An optimal animal model should mimic the human disease process with clinical consistency and efficiency in the short and long terms, and incidence of the disease should be high, with reliable reducibility through an inexpensive method. The LKB1 KO mouse has all of these merits as a small animal model of AF. The spontaneous nature of AF presents the opportunity to study the molecular mechanism of initiation and progression of the disease process. Our model has no alteration of the pathophysiological process by nonphysiological methods or disease conditions to induce AF. Previous reports demonstrated the prevalence of spontaneous AF in 40% to 50% of CREM-transgenic mice at age 14 weeks and in 60% of mice with cardiac-specific overexpression of RhoA.[38,39] We documented higher occurrence of AF (95% at 12 weeks) in LKB1 KO mice. Moreover, this model provides a unique opportunity to study new medications for primary and secondary prevention of AF because LKB1 KO

mice demonstrate all of the stages of AF from SR to PAF and persAF.

LKB1 KO mice demonstrated a very close relationship between electrical and structural remodeling of atria in the process of developing AF. During SR, the LKB1 KO heart has HR and conduction intervals similar to WT, but incidence of AVB and premature atrial and ventricular contractions were higher in parallel with inflammation and initiation of biatrial enlargement. As in humans, AVB and frequent premature atrial contractions are indicators of development of AF.[40,41] Atrial flutter was also seen in our model before progressing to AF or alternating with PAF. As we reported recently,[42] coexistence of AF and atrial flutter are common in humans as a result of diseased atrium.[41] In this study, our findings in the LKB1 KO mouse model of AF are consistent with findings in humans; however, P-wave amplitude and duration were not found to be predictors for initiation of AF despite their predictive value in human AF.[43] Sinus node function and intrinsic HR were normal in KO mice in comparison to WT; therefore, sinus node dysfunction did not contribute to AF in our model. KO mice with persAF have a slower ventricular rate but normal QRS and QTc intervals. Ventricular tachycardia and fibrillation occurred in persAF and resulted in sudden death.

Electrical and structural remodeling trigger each other in AF. Structural remodeling in right and left atria was remarkable in LKB1 KO hearts, as shown. Biatrial enlargement and associated ultrastructural changes started in SR and gradually worsened throughout PAF and persAF. Pathological processes included inflammatory myocarditis, heterogeneous infiltration, apoptosis, necrosis, and fibrosis. There was severe disorganization of extracellular space and deformation of the intracellular myofibrillar structure. KO heart developed dilated atrial cardiomyopathy, which was vulnerable to electrophysiological triggers. Atrial dilation, stretch, fibrosis, loss of muscle mass, and cellular and matrix remodeling and disruption of gap junctions are documented in our model. Initiation and progression of AF are associated with these pathologies and result in a vulnerable atrial substrate with a heterogeneous atrial effective refractory period and conduction velocity. This establishes the interrelation of structural and electrical substrate in AF. Consequently, initiation of PAF and progression to persAF involves an inflammatory process in atrial myocardium.

Although the role of inflammation in AF has been discussed in the literature, there is no clear understanding of the process or evidence of inflammation in the disease pathogenesis.[44,45] In this study, we demonstrated that inflammation was present in the tissue samples of atria before and after the initiation of AF. In addition, systemic inflammatory response was evident with elevated serum biomarkers such as CRP, IL-6, and TNF-α during the initiation and progression of AF. Inflammation was associated with oxidative stress through increased reactive oxygen species generation in LKB1 KO atria. Because LKB1 regulates AMPK activation, we found decreased phosphorylation of AMPKα in our LKB1 KO mice as a reflection of metabolic stress. In association with oxidative and metabolic stress, inflammation is the main contributor to atrial electroanatomical remodeling and atrial cardiomyopathy in the development of AF. This presents a new therapeutic target for prevention or treatment of AF by suppressing inflammation.

Our study demonstrated that AF caused LV systolic dysfunction with depressed LV ejection fraction and clinical heart failure. It is known that heart failure causes AF, and we showed that AF generated heart failure with low LV ejection fraction and clinical signs of congestion including weight gain, edema, reduced daily physical activities, and pleural and pericardial effusion in KO mice. Serial echocardiogram and cardiac MRI showed that LV ejection fraction was reduced after development of persAF; it was not associated with ventricular hypertrophy, as proposed by others.[28] As we showed in this study, mice with AF developed peripartum cardiomyopathy with a high mortality rate. To our knowledge, this study is the first in the literature to report that AF is a risk factor for peripartum cardiomyopathy and increases peripartum mortality. In addition, AF is associated with exercise intolerance and reduced survival. KO mice showed lower workload, with poor exercise capacity on the treadmill. As in patients with AF,[1–9,42] long-term survival was impaired in KO mice with AF. Causes of death included clinical heart failure and sudden death with ventricular tachycardia or fibrillation. Survival in KO mice was long enough to evaluate the effect of new therapeutic agents to prevent AF-related morbidity and mortality.

LKB1 encodes a serine/threonine protein kinase, which functions upstream of the AMPK superfamily.[27,28,46] LKB1 plays a major role in the regulation of cellular metabolism, proliferation, and polarity. Moreover, LKB1/AMPK signaling in cardiac myocytes is essential for normal development of the atria and ventricles. Mitochondria- and AMPK-regulated cardiomyocyte energetics and metabolism have important roles in myocardial structural and electrical remodeling. Consequently, cellular energetics and metabolism may play significant mechanistic roles in initiation and maintenance of AF. Cellular energy current may function as a sensor of oxidative or metabolic stress in the heart and modulate arrhythmia.[29] Cytosolic and mitochondrial energetics, regulated by the mitochondrial inner membrane and the cytosolic AMPK system, could be the center of the AF mechanism. Additional studies are needed to determine further mechanisms causing AF in this model.

In conclusion, the LKB1 KO mouse model of AF is effective and reliable for studying disease mechanisms and new therapies in AF. Lack of LKB1 in mouse heart provokes an

AF phenotype. It accurately represents human AF with characteristic structural and electrical remodeling in atria. Inflammatory atrial myocarditis with progressive atrial cardiomyopathy is the genesis of AF, with characteristic electrical and structural remodeling. Oxidative and metabolic stress contributes to the development of inflammation and AF. Because AF is a progressive disease, primary and secondary prevention of the disease are equally important. Suppression of inflammation and oxidative or metabolic stress is a promising therapeutic target for primary and secondary prevention of AF. The spontaneous nature of AF initiation in the LKB1 KO heart and an appropriate survival rate provide a unique opportunity for further study of molecular mechanisms and novel therapeutic strategies for primary and secondary prevention of AF.

Sources of Funding

This study was supported by the National Institutes of Health/National Heart, Lung, and Blood Institute (Ozcan, grant number 1K08HL117082-01A1).

Disclosures

None.

References

1. January CT, Wann LS, Alpert JS, Calkins H, Cleveland JC Jr, Cigarroa JE, Conti JB, Ellinor PT, Ezekowitz MD, Field ME, Murray KT, Sacco RL, Stevenson WG, Tchou PJ, Tracy CM, Yancy CW. 2014 AHA/ACC/HRS guideline for the management of patients with atrial fibrillation: a report of the American College of Cardiology/American Heart Association Task Force on Practice Guidelines and the Heart Rhythm Society. *Circulation*. 2014;130:2071–2104.
2. Miyasaka Y, Barnes ME, Gersh BJ, Cha SS, Bailey KR, Abhayaratna WP, Seward JB, Tsang TS. Secular trends in incidence of atrial fibrillation in Olmsted County, Minnesota, 1980 to 2000, and implications on the projections for future prevalence. *Circulation*. 2006;114:119–125.
3. Go AS, Hylek EM, Phillips KA, Chang Y, Henault LE, Selby JV, Singer DE. Prevalence of diagnosed atrial fibrillation in adults: national implications for rhythm management and stroke prevention: the anticoagulation and risk factors in atrial fibrillation (ATRIA) Study. *JAMA*. 2001;285:2370–2375.
4. Lloyd-Jones DM, Wang TJ, Leip EP, Larson MG, Levy D, Vasan RS, D'Agostino RB, Massaro JM, Beiser A, Wolf PA, Benjamin EJ. Lifetime risk for development of atrial fibrillation: the Framingham Heart Study. *Circulation*. 2004;110:1042–1046.
5. Kannel WB, Wolf PA, Benjamin EJ, Levy D. Prevalence, incidence, prognosis, and predisposing conditions for atrial fibrillation: population-based estimates. *Am J Cardiol*. 1998;82:2N–9N.
6. Ott A, Breteler MM, de Bruyne MC, de Bruyne MC, van Harskamp F, Grobbee DE, Hofman A. Atrial fibrillation and dementia in a population-based study: the Rotterdam Study. *Stroke*. 1997;28:316–321.
7. Benjamin EJ, Wolf PA, D'Agostino RB, Silbershatz H, Kannel WB, Levy D. Impact of atrial fibrillation on the risk of death: the Framingham Heart Study. *Circulation*. 1998;98:946–952.
8. Wang TJ, Larson MG, Levy D, Vasan RS, Leip EP, Wolf PA, D'Agostino RB, Murabito JM, Kannel WB, Benjamin EJ. Temporal relations of atrial fibrillation and congestive heart failure and their joint influence on mortality: the Framingham Heart Study. *Circulation*. 2003;107:2920–2925.
9. Krahn AD, Manfreda J, Tate RB, Mathewson FA, Cuddy TE. The natural history of atrial fibrillation: incidence, risk factors, and prognosis in the Manitoba Follow-Up Study. *Am J Med*. 1995;98:476–484.
10. Le Heuzey JY, Paziaud O, Piot O, Said MA, Copie X, Lavergne T, Guize L. Cost of care distribution in atrial fibrillation patients: the COCAF study. *Am Heart J*. 2004;147:121–126.
11. Stewart S, Murphy NF, Walker A, McGuire A, McMurray JJ. Cost of an emerging epidemic: an economic analysis of atrial fibrillation in the UK. *Heart*. 2004;90:286–292.
12. Wattigney WA, Mensah GA, Croft JB. Increasing trends in hospitalization for atrial fibrillation in the United States, 1985 through 1999: implications for primary prevention. *Circulation*. 2003;108:711–716.
13. Kannel WB, Abbott RD, Savage DD, McNamara PM. Epidemiologic features of chronic atrial fibrillation: the Framingham Study. *N Engl J Med*. 1982;306:1018–1022.
14. Kannel WB, Abbott RD, Savage DD, McNamara PM. Coronary heart disease and atrial fibrillation: the Framingham Study. *Am Heart J*. 1983;106:389–396.
15. Benjamin EJ, Levy D, Vaziri SM, D'Agostino RB, Belanger AJ, Wolf PA. Independent risk factors for atrial fibrillation in a population-based cohort. The Framingham Heart Study. *JAMA*. 1994;271:840–844.
16. Psaty BM, Manolio TA, Kuller LH, Kronmal RA, Cushman M, Fried LP, White R, Furberg CD, Rautaharju PM. Incidence of and risk factors for atrial fibrillation in older adults. *Circulation*. 1997;96:2455–2461.
17. Lubitz SA, Ozcan C, Magnani JW, Kääb S, Benjamin EJ, Ellinor PT. Advances in the genetics of atrial fibrillation: implications for future research directions and personalized medicine. *Circ Arrhythm Electrophysiol*. 2010;1:291–299.
18. Estes NA III, Sacco RL, Al-Khatib SM, Ellinor PT, Bezanson J, Alonso A, Antzelevitch C, Brockman RG, Chen PS, Chugh SS, Curtis AB, DiMarco JP, Ellenbogen KA, Epstein AE, Ezekowitz MD, Fayad P, Gage BF, Go AS, Hlatky MA, Hylek EM, Jerosch-Herold M, Konstam MA, Lee R, Packer DL, Po SS, Prystowsky EN, Redline S, Rosenberg Y, Van Wagoner DR, Wood KA, Yue L, Benjamin EJ. American Heart Association atrial fibrillation research summit: a conference report from the American Heart Association. *Circulation*. 2011;124:363–372.
19. Allessie MA, Boyden PA, Camm AJ, Kléber AG, Lab MJ, Legato MJ, Rosen MR, Schwartz PJ, Spooner PM, Van Wagoner DR, Waldo AL. Pathophysiology and prevention of atrial fibrillation. *Circulation*. 2001;103:769–777.
20. Nattel S. New ideas about atrial fibrillation 50 years on. *Nature*. 2002;415:219–226.
21. Wakili R, Voigt N, Kääb S, Dobrev D, Nattel S. Recent advances in the molecular pathophysiology of atrial fibrillation. *J Clin Invest*. 2011;121:2955–2968.
22. Nattel S, Burstein B, Dobrev D. Atrial remodeling and atrial fibrillation: mechanisms and implications. *Circ Arrhythm Electrophysiol*. 2008;1:62–73.
23. Nishida K, Michael G, Dobrev D, Nattell S. Animal models for atrial fibrillation: clinical insight and scientific opportunities. *Europace*. 2010;12:160–172.
24. Milan DJ, MacRae CA. Animal models for arrhythmias. *Cardiovasc Res*. 2005;67:426–437.
25. Riley G, Syeda F, Kirchhof P, Fabritz L. An introduction to murine models of atrial fibrillation. *Front Physiol*. 2012;3:296;1–16.
26. Loeb JM, deTarnowsky JM. Acetylcholine-calcium interactions in the canine atrium and sinus node. *Am Heart J*. 1984;107:1161–1168.
27. Ikeda Y, Sato K, Pimentel DR, Sam F, Shaw RJ, Dyck JR, Walsh K. Cardiac-specific deletion of LKB1 leads to hypertrophy and dysfunction. *J Biol Chem*. 2009;284:35839–35849.
28. Nakada D, Saunders TL, Morrison SJ. LKB1 regulates cell cycle and energy metabolism in haematopoietic stem cells. *Nature*. 2010;468:653–658.
29. Ozcan C, Palmeri M, Horvath TL, Horvath TL, Russell KS, Russell RR III. Role of uncoupling protein 3 in ischemia-reperfusion injury, arrhythmias, and preconditioning. *Am J Physiol Heart Circ Physiol*. 2013;304:H1192–H1200.
30. Weiergräber M, Henry M, Südkamp M, de Vivie ER, Hescheler J, Schneider T. Ablation of Ca(v)2.3/E-type voltage-gated calcium channel results in cardiac arrhythmia and altered autonomic control within the murine cardiovascular system. *Basic Res Cardiol*. 2005;100:1–13.
31. da Costa-Goncalves AC, Tank J, Plehm R, Diedrich A, Todiras M, Gollasch M, Heuser A, Wellner M, Bader M, Jordan J, Luft FC, Gross V. Role of the multidomain protein spinophilin in blood pressure and cardiac function regulation. *Hypertension*. 2008;52:702–707.
32. Ludwig A, Budde T, Stieber J, Moosmang S, Wahl C, Holthoff K, Langebartels A, Wotjak C, Munsch T, Zong X, Feil S, Feil R, Lancel M, Chien KR, Konnerth A, Pape HC, Biel M, Hofmann F. Absence epilepsy and sinus dysrhythmia in mice lacking the pacemaker channel HCN2. *EMBO J*. 2003;22:216–224.
33. Rosenberg MA, Das S, Pinzon PQ, Knight AC, Sosnovik DE, Ellinor PT, Rosenzweig A. A novel transgenic mouse model of cardiac hypertrophy and atrial fibrillation. *J Atr Fibrillation*. 2012;2:1–15.

34. Maceira AM, Cosín-Sales J, Roughton M, Prasad SK, Pennell DJ. Reference right atrial dimensions and volume estimation by steady state free precession cardiovascular magnetic resonance. *J Cardiovasc Magn Reson*. 2013;15:29.
35. Ozcan C, Bienengraeber M, Hodgson DM, Mann DL, Terzic A. Mitochondrial tolerance to stress impaired in failing heart. *J Mol Cell Cardiol*. 2003;35:1161–1166.
36. Lynch P, Lee TC, Fallavollita JA, Canty JM Jr, Suzuki G. Intracoronary administration of AdvFGF-5 (fibroblast growth factor-5) ameliorates left ventricular dysfunction and prevents myocyte loss in swine with developing collaterals and ischemic cardiomyopathy. *Circulation*. 2007;116:I71–I76.
37. Hodgson DM, Zingman L, Kane G, Perez-Terzic C, Bienengraeber M, Ozcan C, Gumina RJ, Pucar D, O'Coclain F, Mann DL, Alekseev AE, Terzic A. Cellular remodeling in heart failure disrupt K_{ATP} channel-dependent stress tolerance. *EMBO J*. 2003;22:1732–1742.
38. Nielsen JB, Pietersen A, Graff C, Lind B, Struijk JJ, Olesen MS, Haunsø S, Gerds TA, Ellinor PT, Køber L, Svendsen JH, Holst AG. Risk of atrial fibrillation as a function of the electrocardiographic PR interval: results from the Copenhagen ECG Study. *Heart Rhythm*. 2013;10:1249–1256.
39. Kirchhof P, Marijon E, Fabritz L, Li N, Wang W, Wang T, Schulte K, Hanstein J, Schulte JS, Vogel M, Mougenot N, Laakmann S, Fortmueller L, Eckstein J, Verheule S, Kaese S, Staab A, Grote-Wessels S, Schotten U, Moubarak G, Wehrens XH, Schmitz W, Hatem S, Müller FU. Overexpression of cAMP-response element modulator causes abnormal growth and development of the atrial myocardium resulting in a substrate for sustained atrial fibrillation in mice. *Int J Cardiol*. 2013;166:366–374.
40. Sah VP, Minamisawa S, Tam SP, Wu TH, Dorn GW II, Ross J Jr, Chien KR, Brown JH. Cardiac-specific overexpression of RhoA results in sinus and atrioventricular nodal dysfunction and contractile failure. *J Clin Invest*. 1999;103:1627–1634.
41. Waldo AL, Feld GK. Inter-relationships of atrial fibrillation and atrial flutter mechanisms and clinical implications. *J Am Coll Cardiol*. 2008;51:779–786.
42. Ozcan C, Strom J, Newell J, Mansour M, Ruskin J. Incidence and predictors of atrial fibrillation and its impact on long-term survival in patients with supraventricular arrhythmias. *Europace*. 2014;16:1508–1514.
43. Magnani JW, Johnson VM, Sullivan LM, Gorodeski EZ, Schnabel RB, Lubitz SA, Levy D, Ellinor PT, Benjamin EJ. P wave duration and risk of longitudinal atrial fibrillation in persons $\geq$ 60 years old (from the Framingham Heart Study). *Am J Cardiol*. 2001;107:917–921.
44. Aviles RJ, Martin DO, Apperson-Hansen C, Houghtaling PL, Rautaharju P, Kronmal RA, Tracy RP, Van Wagoner DR, Psaty BM, Lauer MS, Chung MK. Inflammation as a risk factor for atrial fibrillation. *Circulation*. 2003;108:3006–3010.
45. Issac TT, Dokainish H, Lakkis NM. Role of inflammation in initiation and perpetuation of atrial fibrillation: a systematic review of the published data. *J Am Coll Cardiol*. 2007;50:2021–2028.
46. Young LH. AMP-activated protein kinase conducts the ischemic stress response orchestra. *Circulation*. 2008;117:832–840.